L. H. Tong
Department of Modern Mechanics,
University of Science and Technology of China,
Hefei, Anhui 230026, China;
USTC-City University,
Joint Advanced Research Centre,
Suzhou, Jiangsu 215123, China

C. W. Lim[1]
Department of Civil and
Architectural Engineering,
City University of Hong Kong,
Kowloon, Hong Kong SAR, China;
USTC-City University,
Joint Advanced Research Centre,
Suzhou, Jiangsu 215123, China
e-mail: bccwlim@cityu.edu.hk

Y. C. Li
Department of Modern Mechanics,
University of Science and Technology of China,
Hefei, Anhui 230026, China

Gas-Filled Encapsulated Thermal-Acoustic Transducer

A new model for a gas-filled encapsulated thermal-acoustic transducer, which uses newly devised carbon nanotube (CNT) thin film is developed and the exact and approximate solutions are derived. A comparison between theoretical prediction and experimental data is presented and excellent agreement is reported. The frequency response for this acoustic transducer is investigated and the acoustic response of as a function of window–thin-film distance of the encapsulated transducer is discussed. An optimal distance between window and thin film is successfully derived and used in some practical examples. Resonance takes place for a suitable input frequency, and thus such transducers can be used to either generate acoustic waves of specific frequency or to filter specific resonant frequencies from a wide spectrum of signals. This kind of transducer can be immersed in different liquid media. A gaseous medium shows better performance at lower frequency while it is otherwise for a liquid medium. The conclusions derived in this work could be regarded as effective guidelines and information for enhancing thermal-acoustics efficiency conversion, as well as for the optimal design of a thermal-acoustic transducer.
[DOI: 10.1115/1.4024765]

Keywords: carbon nanotube (CNT) thin film, resonance, thermal-acoustics, transducer

1 Introduction

Thermophone, whose mechanism of acoustic generation is different from conventional electro-acoustic devices in which sound is produced by the mechanical vibration [1–4], was first studied by Arnold and Crandall [5] almost a century ago. Because materials with a low heat capacity were unavailable at that time, the acoustic pressure emitted from their thermophone was very small [6]. Owing to rapid advancement of nanotechnology and nanomaterials, in particular the discovery of carbon nanotubes in recent years, thermal-acoustics again attracts wide attention and the subject is undergoing fast development [7]. In 1999, an efficient ultrasound emitter composed of a 30 nm thick aluminum film on a microporous silicon layer (10 mm thick) and a *p*-type crystalline silicon (*c*-Si) wafer was reported by Shinoda et al. [8]. Another recently remarkable discovery by Xiao et al. [6] is the generation of powerful acoustic waves when an alternating current (ac) is applied to a carbon nanotube (CNT) thin film drawn from an array of CNT forests [9]. Aliev et al. [10] conducted the same experiment as that of Xiao et al. [6] but the CNT thin film was placed in a liquid medium. A strong thermal-acoustic response was also detected for an aligned array of multiwalled carbon nanotube (MWCNT) forests by Kozlov et al. [11]. In 2011, a graphene-on-paper thermal-acoustic source was fabricated and tested by Tian et al. [12]. It was also demonstrated that considerable acoustic energy can be emitted from a suspended metal wire array when an alternating current is applied [8,13,14]. The conversion efficiency from electrical power to acoustic power for a thermophone was discussed by Vesterinen et al. [14] and Tian et al. [12]. In addition, Xiao et al. [15] also recorded the thermal-acoustic response in different gaseous media and stated that higher acoustic pressure levels can be achieved in a gaseous medium with smaller heat capacity. All of these thermophones have one common feature, i.e., small heat capacity per unit area for the thermal-acoustic source [13].

Although many experiments were conducted with different pieces of supporting theoretical analysis, the development of a rigorous model based on theoretical analysis has been lacking. In Arnold and Crandall [5], they did not consider the effect of heat capacity per unit area of the thin film. Xiao et al. [6] revised Arnold and Crandall's model but his was only suitable for a far-field response. By applying Green's function, Vesterinen et al. [14] presented an acoustic pressure expression, which considered the effect of a heat-absorbing substrate. Hu et al. [16] explained the experimental results of Shinoda et al. [8] by solving a set of coupled thermal-mechanical equations. Aliev et al. [17] measured the acoustic pressure response for the argon filled encapsulated MWCNT transducer but they did not present any theoretical analysis or explanation.

In this paper, a rigorous analytical model with theoretical formulation for a gas-filled encapsulated thermal-acoustic transducer which uses nanotube thin film is first proposed and a set of thermal-mechanical coupled equations is solved. Exact and approximate solutions are presented and the theoretical prediction compares well with the experimental results of Aliev et al. [17]. The transducer frequency response is analyzed and the influence of the distance between the nanotube thin film and the window of the encapsulated transducer is discussed. Finally, the acoustical response for a transducer immersed in different media is investigated.

2 Theoretical Model and the Solution

The diagram of a gas-filled encapsulated thermal-acoustic transducer is shown in Fig. 1. Gas is channeled into the chamber and a nanotube thin film is suspended in the middle of two windows, which are separated by the spacers. The chamber is sealed carefully with silicon paste or epoxy sealant on the edges. In order to eliminate the influence of reflected sound, the window on the left is made of soundproof material, such as aluminum foam. The distance between the left window and the nanotube thin film is large enough to ensure no influence of sound generated in the left-hand side of the chamber to the acoustic pressure on right-hand side of the nanotube thin film $x > 0$ m. Therefore only the right-hand side of the nanotube thin film is considered.

Upon applying an alternating current to the nanotube thin film in the encapsulated chamber, gas near the thin film is heated in a harmonic manner with respect to the period of current. Thus, the gas expands and contracts sinusoidally and sound is emitted from the chamber outwards through the window. Here, a one-dimensional treatment of the thermal and acoustic processes in the

[1]Corresponding author.

Contributed by the Noise Control and Acoustics Division of ASME for publication in the JOURNAL OF VIBRATION AND ACOUSTICS. Manuscript received April 07, 2013; final manuscript received May 15, 2013; published online July 5, 2013. Assoc. Editor: Theodore Farabee.

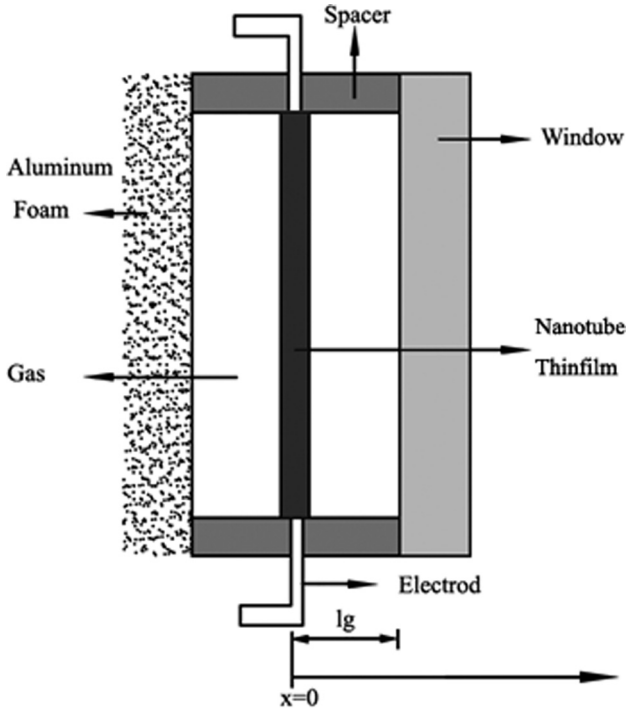

Fig. 1 The cross section of the gas-filled encapsulated thermal-acoustic transducer with nanotube thin film

chamber is considered. Because window–thin-film distance is small, the acoustic wave could be considered as a plane wave [18]. The coupled governing linear equations for time-dependent acoustic pressure and temperature are [19]

$$\begin{cases} \dfrac{\partial^2 p_g}{\partial t^2} - C_T^2 \dfrac{\partial^2 p_g}{\partial x^2} = \dfrac{\rho_g C_T^2}{T_m} \dfrac{\partial^2 T_g}{\partial t^2} \\ \dfrac{\partial T_g}{\partial t} - \alpha_g \dfrac{\partial^2 T_g}{\partial x^2} = \dfrac{\alpha_g}{\kappa_g} \dfrac{\partial p_g}{\partial t} \end{cases} \tag{1}$$

where ρ_g is gas density, p_g is gas pressure, $C_T = P_0/\rho_0$ is defined as the isothermal sound velocity in gas, ρ_0 is the reference gas density, P_0 is the ambient pressure, t is time, T_g and T_m are varying temperature and average temperature in the chamber, respectively, α_g is the coefficient of thermal diffusivity in gas, and κ_g is the thermal conductivity of gas. For an alternating current with frequency $\omega/2$, the fundamental equation for the heated nanotube thin film is [20]

$$P_{\text{in}} - P_{\text{in}} e^{j\omega t} = 2s\beta_0 T_f + 2sQ_0 + sc_s \frac{dT_f}{dt} \tag{2}$$

where P_{in} is the input power, β_0 is rate of heat loss per unit area, s is the single-side area of the thin film, c_s is heat capacity per unit area, T_f is temperature above its surroundings, and

$$Q_0 = -\kappa_g \left.\frac{\partial T_g(x,t)}{\partial x}\right|_{x=0}$$

is instantaneous heat flow per unit area from the thin film to the surrounding medium. Assuming $p_g(x,t) = \bar{p}_g(x)\exp(j\omega t)$, $T_g(x,t) = \bar{T}_g(x)\exp(j\omega t)$, $T_f(t) = T_a + \bar{T}_f \exp(j\omega t)$, and substituting these expressions into Eqs. (1) and (2), the governing equations for the complex-amplitudes $\bar{p}_g(x)$, $\bar{T}_g(x)$, and $\bar{T}_f$ can be obtained as

$$\frac{d^2\bar{p}_g}{dx^2} + \frac{\omega^2}{C_T^2}\bar{p}_g = \frac{\rho_g \omega^2}{T_m}\bar{T}_g \tag{3}$$

$$\alpha_g \frac{d^2\bar{T}_g}{dx^2} - j\omega\bar{T}_g = -\frac{j\omega}{\rho_g C_P}\bar{P}_g \tag{4}$$

$$P_{\text{in}} - P_{\text{in}}\exp(j\omega t) = 2s\beta_0 T_a + \left(2s\beta_0\bar{T}_f - 2s\kappa_g \left.\frac{d\bar{T}_g}{dx}\right|_{x=0} + j\omega s c_s \bar{T}_f\right) \times \exp(j\omega t) \tag{5}$$

where γ is the heat capacity ratio of gas. Defining a set of notations as $a = j\omega/\alpha_g$, $b = -j\omega/\kappa_g$, $c = \rho_g\omega^2/T_m$, $d = -\omega^2/C_T^2$, $\sigma_1^2 = \left[a + d + \sqrt{(a+d)^2 - 4(ad-bc)}\right]/2$, $\sigma_2^2 = [a + d - \sqrt{(a+d)^2 - 4(ad-bc)}]/2$, then the combination of Eqs. (3) and Eq. (4) gives

$$\bar{T}_g(x) = C_1\exp(-\sigma_1 x) + C_2\exp(\sigma_1 x) + C_3\exp(-\sigma_2 x) + C_4\exp(\sigma_2 x) \quad \text{for} \quad 0 < x < l_g \tag{6}$$

$$\bar{p}_g(x) = d_1[C_1\exp(-\sigma_1 x) + C_2\exp(\sigma_1 x)] + d_2[C_3\exp(-\sigma_2 x) + C_4\exp(\sigma_2 x)] \quad \text{for} \quad 0 < x < l_g \tag{7}$$

in which $d_1 = (\sigma_1^2 - a)/b$, $d_2 = (\sigma_2^2 - a)/b$, and $C_i (i = 1,2,3,4)$ are the undetermined constant coefficients which could be determined from the boundary conditions.

The harmonically varying temperature is effectively and completely damped out at a distance of $2\pi\mu_g$ in the gas, where $\mu_g = \sqrt{2\alpha_g/\omega}$ is the thermal diffusion length [21]. For a given length $l_g < 2\pi\mu_g$, it is possible for the thermal wave to penetrate into the window; as a result, the thermal properties of the window influence the acoustic signals. Otherwise, there is no influence for $l_g > 2\pi\mu_g$. Hence, two separate cases are discussed.

2.1 Window Independent Region $l_g > 2\pi\mu_g$. The temperature effect does not reach the inner side of the window and hence the thermal wave does not propagate in the window. The thermal and mechanical boundary conditions at $x = 0$ and $x = l_g$ are

$$\begin{aligned} &\frac{d\bar{p}_g}{dx} = 0; \qquad \bar{T}_g = \bar{T} \quad \text{at} \quad x = 0 \\ &\frac{d\bar{p}_g}{dx} = 0; \qquad \bar{T}_g = 0 \quad \text{at} \quad x = l_g \end{aligned} \tag{8}$$

There are four boundary conditions and four undetermined coefficients, thus the equation is deterministic. Substitute Eqs. (6) and (7) into the boundary conditions and a set of equations for $C_i (i = 1,2,3,4)$ is obtained as

$$\begin{bmatrix} 1 & 1 & 1 & 1 \\ -d_1\sigma_1 & d_1\sigma_1 & -d_2\sigma_2 & d_2\sigma_2 \\ \exp(-\sigma_1 l_g) & \exp(\sigma_1 l_g) & \exp(-\sigma_2 l_g) & \exp(\sigma_2 l_g) \\ -d_1\sigma_1\exp(-\sigma_1 l_g) & d_1\sigma_1\exp(\sigma_1 l_g) & -d_2\sigma_2\exp(-\sigma_2 l_g) & d_2\sigma_2\exp(\sigma_2 l_g) \end{bmatrix} \begin{pmatrix} C_1 \\ C_2 \\ C_3 \\ C_4 \end{pmatrix} = \begin{pmatrix} \bar{T}_f \\ 0 \\ 0 \\ 0 \end{pmatrix} \tag{9}$$

For brevity and convenience, the following notations are introduced:

$$M = d_1\sigma_1, \quad N = d_2\sigma_2, \quad E_1 = \exp(\sigma_1 l_g), \quad E_2 = \exp(\sigma_2 l_g) \tag{10}$$

then Eq. (9) is simplified as

$$\begin{bmatrix} 1 & 1 & 1 & 1 \\ -M & M & -N & N \\ 1/E_1 & E_1 & 1/E_2 & E_2 \\ -M/E_1 & ME_1 & -N/E_2 & NE_2 \end{bmatrix} \begin{pmatrix} C_1 \\ C_2 \\ C_3 \\ C_4 \end{pmatrix} = \begin{pmatrix} \bar{T}_f \\ 0 \\ 0 \\ 0 \end{pmatrix} \tag{11}$$

Introducing eight new notations as follows:

$$\begin{aligned} R_1 &= \frac{1}{2}\left(1 - \frac{N}{M}\right)(1 - E_1^2) + \frac{E_1}{E_2} - 1 \\ R_2 &= \frac{1}{2}\left(1 + \frac{N}{M}\right)(1 - E_1^2) + E_1E_2 - 1 \\ Q_1 &= \left(1 - \frac{N}{M}\right)\left(\frac{1}{E_2} - E_1\right) \\ Q_2 &= \left(1 + \frac{N}{M}\right)(E_2 - E_1) \\ D_1 &= -\frac{1}{2}(1 + E_1^2), \quad F_1 = -E_1 \\ W_3 &= \frac{D_1Q_2 - F_1R_2}{R_1Q_2 - R_2Q_1}, \quad W_4 = \frac{D_1Q_1 - F_1R_1}{R_1Q_2 - R_2Q_1} \end{aligned} \tag{12}$$

allows Eq. (11) to be simplified to

$$\begin{bmatrix} 1 & 1 & 1 & 1 \\ 0 & 2 & 1 - \frac{N}{M} & 1 + \frac{N}{M} \\ 0 & 0 & R_1 & R_2 \\ 0 & 0 & Q_1 & Q_2 \end{bmatrix} \begin{pmatrix} C_1 \\ C_2 \\ C_3 \\ C_4 \end{pmatrix} = \bar{T}_f \begin{pmatrix} 1 \\ 1 \\ D_1 \\ F_1 \end{pmatrix} \tag{13}$$

The solution to Eq. (13) is

$$C_1 = W_1\bar{T}_f, \quad C_2 = W_2\bar{T}_f, \quad C_3 = W_3\bar{T}_f, \quad C_4 = W_4\bar{T}_f \tag{14}$$

where

$$\begin{aligned} W_1 &= \frac{1}{2}\left[1 - (W_3 + W_4) - \frac{N}{M}(W_3 - W_4)\right] \\ W_2 &= \frac{1}{2}\left[1 - (W_3 + W_4) + \frac{N}{M}(W_3 - W_4)\right] \end{aligned} \tag{15}$$

Substituting Eq. (14) into Eq. (6) yields

$$\begin{aligned} Q_0 &= -\kappa_g \left.\frac{dT_g}{dx}\right|_{x=0} \\ &= \kappa_g(\sigma_1W_1 - \sigma_1W_3 + \sigma_2W_2 - \sigma_2W_4)\bar{T}_f \cdot \exp(j\omega t) \end{aligned} \tag{16}$$

Then substituting Q_0 into Eq. (5) gives

$$\begin{aligned} T_a &= \frac{P_{\text{in}}}{2s\beta_0} \\ T_f &= \frac{-P_{\text{in}}}{2s} \frac{1}{\beta_0 - \kappa_g\left(j\frac{\omega}{C_0} - \frac{N}{M}\sqrt{j\frac{\omega}{\alpha_g}}\right)(W_4 - W_3) + j\frac{1}{2}\omega c_s} \end{aligned} \tag{17}$$

Combining Eqs. (7),(14), and (17), the exact expressions for acoustic pressure can be obtained. However, these expressions are still too complicated to allow convenient analysis. When $\omega \ll P_0/(\rho_0\alpha_g)$, substituting all known constant parameters into a, b, c, d yields $a \gg d$. Hence, for this case [18,22]

$$\begin{aligned} \sigma_1^2 &\approx a + (\gamma - 1)\sigma_2^2 \\ \sigma_2^2 &\approx d/\gamma \\ d_1 &= (\gamma - 1)d/\gamma b \\ d_2 &= (d/\gamma - a)/b \end{aligned} \tag{18}$$

and furthermore,

$$\begin{aligned} |d_1| &\ll |d_2| \\ |d_1\sigma_1| &\ll |d_2\sigma_2| \end{aligned} \tag{19}$$

or $|N| \gg |M|$ can be deduced. For $l_g > 2\pi\mu_g$, we have $E_1 > 7228.35\exp(\sqrt{j})$ and $E_1 \gg E_2$. For further simplification, the following approximate expressions can be obtained:

$$\begin{aligned} D_1Q_2 - F_1R_2 &\approx -\frac{1}{2}\frac{N}{M}E_1^2E_2 \\ F_1R_1 - D_1Q_1 &\approx -\frac{1}{2}\frac{N}{M}\frac{E_1^2}{E_2} \\ R_1Q_2 - R_2Q_1 &\approx \frac{1}{2}\left(\frac{N}{M}\right)^2 E_1^2\frac{E_2^2 - 1}{E_2} \\ W_3 &= \frac{D_1Q_2 - F_1R_2}{R_1Q_2 - R_2Q_1} \approx -\frac{M}{N}\frac{E_2^2}{E_2^2 - 1} \\ W_4 &= \frac{D_1Q_1 - F_1R_1}{R_1Q_2 - R_2Q_1} \approx -\frac{M}{N}\frac{1}{E_2^2 - 1} \\ W_4 - W_3 &\approx \frac{M}{N} \qquad W_4 + W_3 \approx -\frac{M}{N}\frac{E_2^2 + 1}{E_2^2 - 1} \end{aligned} \tag{20}$$

Based on the simplified expression in Eq. (20), $\bar{T}_f$ can be expressed as

$$\bar{T}_f = \frac{-P_{\text{in}}}{2s} \frac{1}{\beta_0 + \kappa_g\sqrt{j\frac{\omega}{\alpha_g}} + j\frac{1}{2}\omega c_s} \tag{21}$$

and $d_1W_1 \ll d_2W_3, d_1W_1 \ll d_2W_4, d_1W_2 \ll d_2W_3, d_1W_2 \ll d_2W_4$. Thus, the first two terms in Eq. (7) are omitted and the approximate acoustic pressure can be expressed as

$$\begin{aligned} \bar{p}_g(x) = \frac{P_{\text{in}}}{2s} & \frac{\gamma - 1}{\left(\beta_0 + \kappa_g\sqrt{\frac{\omega}{2\alpha_g}}\right) + j\left(\kappa_g\sqrt{\frac{\omega}{2\alpha_g}} + \frac{1}{2}\omega c_s\right)} \\ & \times \sqrt{\frac{j\omega}{\alpha_g}}\frac{\kappa_g}{C_0}\left(\frac{\exp(2k_gl_g)}{\exp(2k_gl_g) - 1}\exp(-k_gx) + \frac{1}{\exp(2k_gl_g) - 1}\right. \\ & \left. \times \exp(k_gx)\right) \end{aligned} \tag{22}$$

for $0 < x < l_g$, where C_0 is the isentropic velocity in gas and $k_g = j\omega/C_0$. It can be seen that the second term in the brackets decreases with the increasing l_g while the first term tends to 1.

2.2 Window Dependent Region $l_g < 2\pi\mu_g$. The temperature affects the window and the thermal wave in the window needs to

be considered. The thermal conductivity equation for the window is

$$\frac{\partial T_s}{\partial t} - \alpha_s \frac{\partial^2 T_s}{\partial x^2} = 0 \tag{23}$$

Assuming a relatively thick window which prevents the thermal wave to penetrate through the window, ensures there is no thermal wave reflection in the window. The solution to Eq. (23) can be obtained by assuming $T_s(x,t) = \bar{T}_s(x)\exp(-j\omega t)$ as [23]

$$\bar{T}_s = C_5 \exp\left(k_s(l_g - x)\right) \qquad \left(l_g < x < l_g + L\right) \tag{24}$$

where C_5 is the undetermined coefficient and L is the thickness of the window. There are five boundary conditions for determining the five coefficients $C_i (i = 1, 2, \ldots, 5)$,

$$\begin{aligned} &\frac{d\bar{p}_g}{dx} = 0; \qquad \bar{T}_g = \bar{T}_f && \text{at} \quad x = 0 \\ &\frac{d\bar{p}_g}{dx} = 0; \qquad \bar{T}_g = \bar{T}; \qquad \kappa_g \frac{d\bar{T}_g}{dx} = \kappa_s \frac{d\bar{T}_s}{dx} && \text{at} \quad x = l_g \end{aligned} \tag{25}$$

Substituting Eqs. (6) and (7) into the boundary conditions in Eq. (25) and eliminating C_5 yields the equation for the undetermined coefficients $C_i (i = 1, 2, 3, 4)$ as

$$\begin{bmatrix} 1 & 1 & 1 & 1 \\ -d_1\sigma_1 & d_1\sigma_1 & -d_2\sigma_2 & d_2\sigma_2 \\ \left(\kappa_s k_s - \kappa_g k_g^*\right)\exp(-\sigma_1 l_g) & \left(\kappa_s k_s + \kappa_g k_g^*\right)\exp(\sigma_1 l_g) & \left(\kappa_s k_s - \kappa_g k_g\right)\exp(-\sigma_2 l_g) & \left(\kappa_s k_s + \kappa_g k_g\right)\exp(\sigma_2 l_g) \\ -d_1\sigma_1\exp(-\sigma_1 l_g) & d_1\sigma_1\exp(\sigma_1 l_g) & -d_2\sigma_2\exp(-\sigma_2 l_g) & d_2\sigma_2\exp(\sigma_2 l_g) \end{bmatrix} \begin{pmatrix} C_1 \\ C_2 \\ C_3 \\ C_4 \end{pmatrix} = \begin{pmatrix} \bar{T}_f \\ 0 \\ 0 \\ 0 \end{pmatrix} \tag{26}$$

where $k_g^* = \sqrt{j\omega/\alpha_g}$ and $k_s = \sqrt{j\omega/\alpha_s}$. Using the notations defined in Eq. (10), Eq. (26) is simplified as

$$\begin{bmatrix} 1 & 1 & 1 & 1 \\ -M & M & -N & N \\ (1-A)/E_1 & (1+A)E_1 & (1-B)/E_2 & (1+B)E_2 \\ -M/E_1 & ME_1 & -N/E_2 & NE_2 \end{bmatrix} \times \begin{pmatrix} C_1 \\ C_2 \\ C_3 \\ C_4 \end{pmatrix} = \begin{pmatrix} \bar{T}_f \\ 0 \\ 0 \\ 0 \end{pmatrix} \tag{27}$$

where $A = \kappa_g k_g^*/\kappa_s k_s, B = \kappa_g k_g/\kappa_s k_s$. The following notations are defined in order to express concisely the solution to Eq. (27),

$$\begin{aligned} A_1 &= \frac{1+A}{1-A}, \quad A_2 = \frac{1-B}{1-A}, \quad A_3 = \frac{1+B}{1-A}, \\ G_1 &= \frac{1}{2}A_1E_1^2\left(\frac{N}{M}-1\right) - \frac{1}{2}\left(\frac{N}{M}+1\right) + A_2\frac{E_1}{E_2} - 1, \\ G_2 &= -\frac{1}{2}A_1E_1^2\left(\frac{N}{M}+1\right) + \frac{1}{2}\left(\frac{N}{M}-1\right) + A_3E_1E_2, \\ H_1 &= \frac{1}{2E_1}\left(\frac{N}{M}+1\right) + \frac{1}{2}\left(\frac{N}{M}-1\right)E_1 - \frac{N}{M}\frac{1}{E_2}, \\ H_2 &= -\frac{1}{2}\left(\frac{N}{M}+1\right)E_1 + \frac{1}{2}\left(1-\frac{N}{M}\right)\frac{1}{E_1} + \frac{N}{M}E_2, \\ D_2 &= -\frac{1}{2}\left(1+A_1E_1^2\right), \qquad F_2 = -\frac{1}{2}\left(E_1 - \frac{1}{E_1}\right), \\ S_3 &= \frac{D_2H_2 - F_2G_2}{G_1H_2 - G_2H_1}, \qquad S_4 = \frac{D_2H_1 - F_2G_1}{G_1H_2 - G_2H_1} \end{aligned} \tag{28}$$

Then the solution to Eq. (27) can be expressed as

$$C_1 = S_1\bar{T}_f, \quad C_1 = S_2\bar{T}_f, \quad C_3 = S_3\bar{T}_f, \quad C_4 = S_4\bar{T}_f \tag{29}$$

where

$$\begin{aligned} S_1 &= \frac{1}{2}\left[1 - (S_3 + S_4) - \frac{N}{M}(S_3 - S_4)\right], \\ S_2 &= \frac{1}{2}\left[1 - (S_3 + S_4) + \frac{N}{M}(S_3 - S_4)\right] \end{aligned} \tag{30}$$

Combining Eqs. (5),(6), and (29), $\bar{T}_f$ and T_a can be obtained and the expressions are similar to Eq. (17) except that W_3, W_4 should be replaced by S_3, S_4. Even with these parameters determined, the expressions are again too complicated to analyze. An approximate simplified expression should be derived. Using the approximate expressions for $d_1, d_2, \sigma_1, \sigma_2, N, M$ derived previously, the following approximations are obtained:

$$\begin{aligned} S_3 &\approx \frac{M}{N}\frac{-A_1E_2^2 + E_2/E_1 - E_2^2/E_1^2}{A_1E_2^2 - A_1 + 1/E_1^2 - E_2^2/E_1^2} \\ S_4 &\approx \frac{M}{N}\frac{-A_1 + A_1E_2/E_1 - 1/E_1^2}{A_1E_2^2 - A_1 + 1/E_1^2 - E_2^2/E_1^2} \\ S_4 - S_3 &\approx \frac{M}{N}\frac{A_1E_1^2\left(E_2^2 - 1\right) + E_1E_2(A_1 - 1)}{A_1E_1^2E_2^2 - A_1E_1^2 + 1 - E_2^2} \\ S_4 + S_3 &\approx \frac{M}{N}\frac{-A_1E_1^2\left(E_2^2 + 1\right) + E_1E_2(1 + A_1)}{A_1E_1^2E_2^2 - A_1E_1^2 + 1 - E_2^2} \end{aligned} \tag{31}$$

From Eq. (31), it is concluded $E_1 > 16.8\exp(\sqrt{j})$ for $l_g > 2\mu_g$ and similar approximate expressions as Eq. (20) could be obtained with W_3, W_4 replaced by S_3, S_4. Therefore the window influences the acoustic pressure significantly only when $l_g < 2\mu_g$. Further analyzing d_1S_1 and d_1S_2 yields the following inequalities:

$$\begin{aligned} d_1S_1 &\ll d_2S_3 \\ d_1S_1 &\ll d_2S_4 \\ d_1S_2 &\ll d_2S_3 \\ d_1S_2 &\ll d_2S_4 \end{aligned} \tag{32}$$

Hence, the first two terms in Eq. (7) can be omitted and the final expression for pressure is

$$\bar{p}_g(x) \approx \frac{P_{\text{in}}}{2s} \frac{1}{\beta_0 + \kappa_g \sqrt{j\frac{\omega}{\alpha_g}} \frac{N}{M}(S_4 - S_3) + j\frac{1}{2}\omega c_s} \left[d_2 S_3 \exp(-k_g x) + d_2 S_4 \exp(k_g x) \right] \tag{33}$$

for $0 < x < l_g$. Acoustic pressure in the chamber is expressed in Eqs. (22) and (33). The acoustic pressure outside of the chamber is the superposition of two acoustic waves, one is sound in the chamber transmitted through the window, and the other is sound generated from window vibration. These two parts of acoustic pressure are obtained separately as follows.

2.3 Sound Transmission Through the Window. Because of the small window–thin-film distance, the acoustic wave in the chamber is mainly a plane wave and the only normal incidence of sound onto the window is considered. The discussion related to sound transmission is presented in Appendix A. From Eqs. (22) and (33), it is clear that there are two sets of pressure waves, i.e., one related to $\exp(-\sigma_2 x)$ which propagates in the positive direction, and the other related to $\exp(\sigma_2 x)$ which propagates in the negative direction. Only the one which propagates towards the positive direction will transmit through the window. Thus, acoustic transmission through the window can be expressed, for $x > l_g + L$ as

$$\bar{p}_{gt}(x) = \begin{cases} \dfrac{P_{\text{in}}}{2s} \dfrac{(\gamma-1)\sqrt{\frac{j\omega}{\alpha_g}} \frac{\kappa_g}{C_0} \frac{\exp(k_g l_g)}{\exp(2k_g l_g) - 1} T \exp\left(j\frac{\omega}{C_m}(L + l_g - x)\right)}{\left(\beta_0 + \kappa_g \sqrt{\frac{\omega}{2\alpha_g}}\right) + j\left(\kappa_g \sqrt{\frac{\omega}{2\alpha_g}} + \frac{1}{2}\omega c_s\right)} & \text{for} \quad l_g > 2\pi\mu_g \\ \dfrac{P_{\text{in}}}{2s} \dfrac{d_2 S_3 T \exp\left(j\frac{\omega}{C_m}(L + l_g - x) - k_g l_g\right)}{\beta_0 + \kappa_g \sqrt{j\frac{\omega}{\alpha_g}} \frac{N}{M}(S_4 - S_3) + j\frac{1}{2}\omega c_s} & \text{for} \quad l_g < 2\pi\mu_g \end{cases} \tag{34}$$

where L is the thickness of the window, C_m is the isentropic sound velocity in the medium outside the chamber, and T is the sound transmission coefficient of the window (see Appendix A).

2.4 Sound Generated From Window Vibration. Forced vibration of the window occurs when a harmonic acoustic pressure expressed in Eq. (22) or Eq. (33) is applied on the inner side of the window. It should be noted that the average chamber temperature increases with increasing electrical power upon applying an alternating current to the nanotube thin film [10]. At the same time, there exists an additional constant pressure which is imposed to the window owing to an increase in temperature. Since silicon paste or epoxy sealant used to seal the window and spacer is soft, the vibrating window could be considered to have non-fully clamped, elastically restrained boundary conditions with torsional stiffness [24]. For simplicity, simply support boundary conditions are assumed and more specific boundary conditions could be investigated at a later stage. The window could then be viewed as a simple support plate with simultaneous constant and harmonic pressure loadings. The acoustic pressure generated from window vibration is (see Appendix B),

$$\bar{p}_{vp}(x) = \frac{64\rho_m C_m}{\rho_w L \pi^4} \sum_{m=1,3,\ldots}^{\infty} \sum_{n=1,3,\ldots}^{\infty} \frac{j\omega \bar{p}_g(l_g)}{m^2 n^2 (\omega_{mn}^2 - \omega^2)} \times \exp\left(j\frac{\omega}{C_m}(l_g + L - x)\right) \tag{35}$$

where ρ_m is the density of the medium with which the transducer is immersed, ρ_w is the density of the window, L is the window thickness, and ω_{mn} is the natural frequency for mode (m, n).

The acoustic pressure outside the chamber is the superposition of sound transmission and the sound generated by window vibrations is

$$\bar{p}_m(x) = \bar{p}_{vp}(x) + \bar{p}_{gt}(x) \tag{36}$$

It should be noted that Eq. (36) is a near-field plane wave. When sound propagates far enough away from the window, it becomes a spherical wave and the acoustic pressure expression should be revised. In this paper, the analysis focuses on the plane wave. In addition, when using Eq. (36) to calculate the acoustic pressure outside the chamber, the thermal length and the window–thin-film distance should always be compared in order to choose an appropriate equation for calculating the acoustic pressure inside the chamber.

3 Numerical Results and Discussion

In this section, numerical examples for an argon-filled encapsulated chamber are presented. The chamber is placed in an open space in air. Different types of window are studied and analytical predictions are compared with published experimental data [17]. The rectangular windows are made of titanium foil and silicon wafer. The nanotube thin films used are MWCNT sheets and different window–thin-film distances are studied. All constant parameters required in Eq. (36) to determine the acoustic pressure are presented in Tables 1 and 2. Although it varies for different input powers [15], the rate of heat loss per unit area β_0 is taken as $15\,\text{W K}^{-1}\text{m}^{-2}$ because it does not significantly influence the acoustic pressure. In addition, because the CNT thin film is placed in an encapsulated chamber, convection loss may be small as

Table 1 Constants used in the analysis for $T = 300$ K

	ρ_0 (kg/m^3)	C_p (JK^{-1}/m^3)	κ (W/mK)	C_0 (m/s)	α (m^2/s)	γ
Air[a]	1.16	1006	0.0262	347	2.25×10^{-5}	1.4
Argon[a]	1.6225	520.34	0.0178	323	2.06×10^{-5}	1.664
Water[b]	1000	—	—	1484	—	—
Methanol[b]	792	—	—	1143	—	—

[a]Reference [15].
[b]Reference [10].

Table 2 Mechanical and thermal properties of window

	E (GPa)	ρ_0 (kg/m^3)	υ	C_0 (m/s)	κ (W/mK)	α (m^2/s)
Titanium[a]	116	4500	0.33	5000	21.9	9.3×10^{-6}
Silicon wafer[b]	129–186	2330	0.22–0.28	7470–8935	141.2	8.66×10^{-5}

[a]Reference [25].
[b]Reference [26].

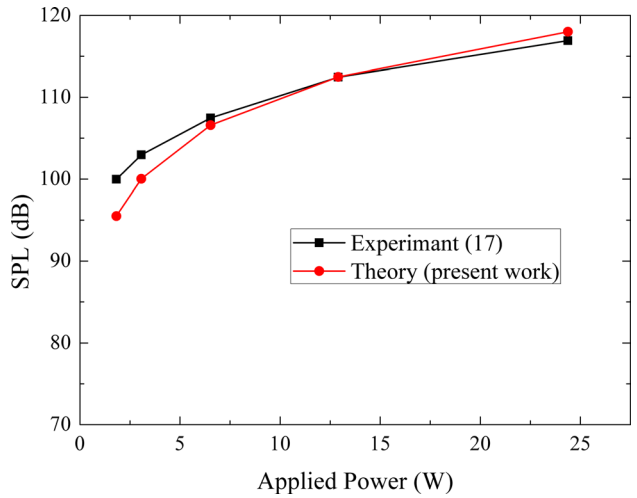

Fig. 2 Acoustic pressure of encapsulated thermal-acoustic transducer fabricated using a 125 μm thick titanium window at frequency of 1500 Hz for different applied powers

compared to radiation loss. As the heat loss is mainly attributed to radiation loss, the lower limit of β_0 is taken in this paper. The heat capacity per unit area $c_s = 7.7 \times 10^{-3}$J/m^{2}K as proposed by Xiao et al. [6] is adopted. The variation of average temperature for varying applied power is omitted when computing acoustic pressure in the chamber and a constant average temperature $T = 300$ K is assumed in the examples.

The first example is a titanium window encapsulated chamber. The experimental results [17] relate the efficiency to input electrical power, which is rather inconvenient for comparison. Instead the results are converted to the efficiency of acoustic pressure outside the chamber and the comparison is shown in Fig. 2. The thickness of the titanium window is 125 μm and the applied frequency is 1500 Hz. The distance between the MWCNT sheet and the window separated by the ceramic spacer is 0.64 mm [17]. The window area is 7.5 cm × 6.5 cm, which is the same as the MWCNT sheet area. The thermal length at 1500 Hz is 0.41 mm, hence, $l_g > 2\pi\mu_g$. From Fig. 2, it can be observed the analytical predictions are in very good agreement with experimental results. The error does not exceed 5% and the maximum error occurs at a low input power of 1.8 W. At this low applied power, the average temperature increase in the chamber is not high enough to induce a significant constant pressure on the window. Hence, the acoustic pressure due to window forced vibration is significant as compared to the pressure contributed by sound transmission. Due to the different assumption of window boundary conditions with respect to the actual experimental conditions, a slight error occurs at this low applied power. At higher applied powers, the chamber average temperature increases with increasing applied power; thus a higher constant pressure on the window exists which increasingly suppresses the window forced vibration. Hence, the acoustic pressure contributed by window vibration becomes increasingly insignificant.

In a second example, the efficiency and acoustic pressure for a silicon wafer window are investigated. The dimensions of this chamber are those of Aliev et al. [17]. It can be deduced that $l_g < 2\pi\mu_g$ at a frequency of 1400 Hz. A comparison of the analytical predictions with experiment is shown in Fig. 3. The efficiency

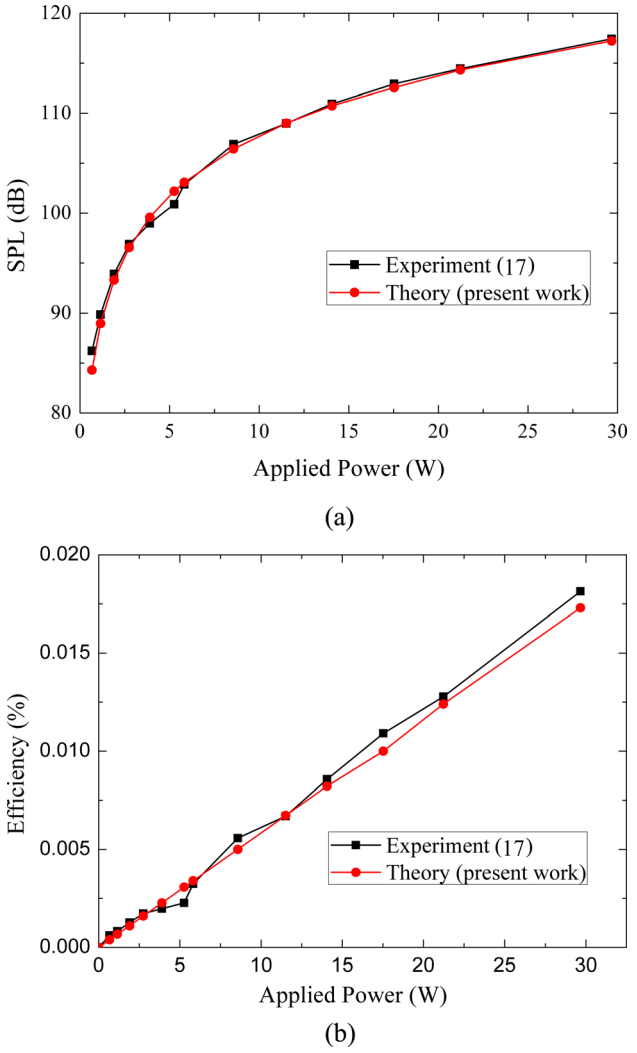

Fig. 3 (*a*) Acoustic response and (*b*) conversion efficiency for an encapsulated thermal-acoustic transducer composed of a 0.75 mm thick silicon wafer window at frequency of 1400 Hz for different applied powers. The silicon wafer window area is 8 cm × 6 cm and the window–MWCNT sheet distance is 0.25 mm.

is $2s(p_{\text{rms}}^2/\rho_0 C_0)/P_{\text{in}}$ [10], in which p_{rms} is the root mean square of acoustic pressure, ρ_0 is the air density, and C_0 is the acoustic velocity in air. From Fig. 3, again excellent agreement between the analytical prediction and experiment is achieved. The transducer energy efficiency is linearly dependent on the input power as shown in Fig. 3(*b*). The efficiency reaches 0.017% which is a high conversion efficiency with respect to the mechanically driven acoustic transducers [24]. The acoustic pressure approaches 117 dB which is significantly higher than that for an applied power of 39.6 W to conventional transducers.

In another example, the frequency response for an argon-filled encapsulated chamber transducer with a window made of titanium and silicon wafer is shown in Fig. 4. The windows are 125μm thick and the input electrical power is 1 W. The area is

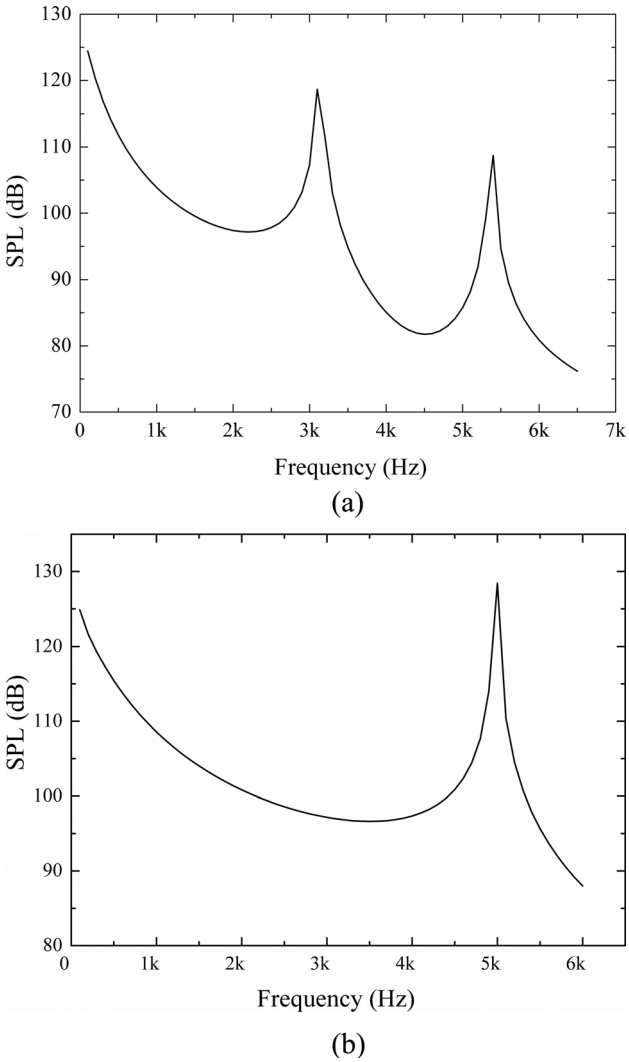

Fig. 4 Frequency response of the argon-filled encapsulated chamber transducer (*a*) titanium window and (*b*) silicon wafer window. The measured points are within the range of a plane wave.

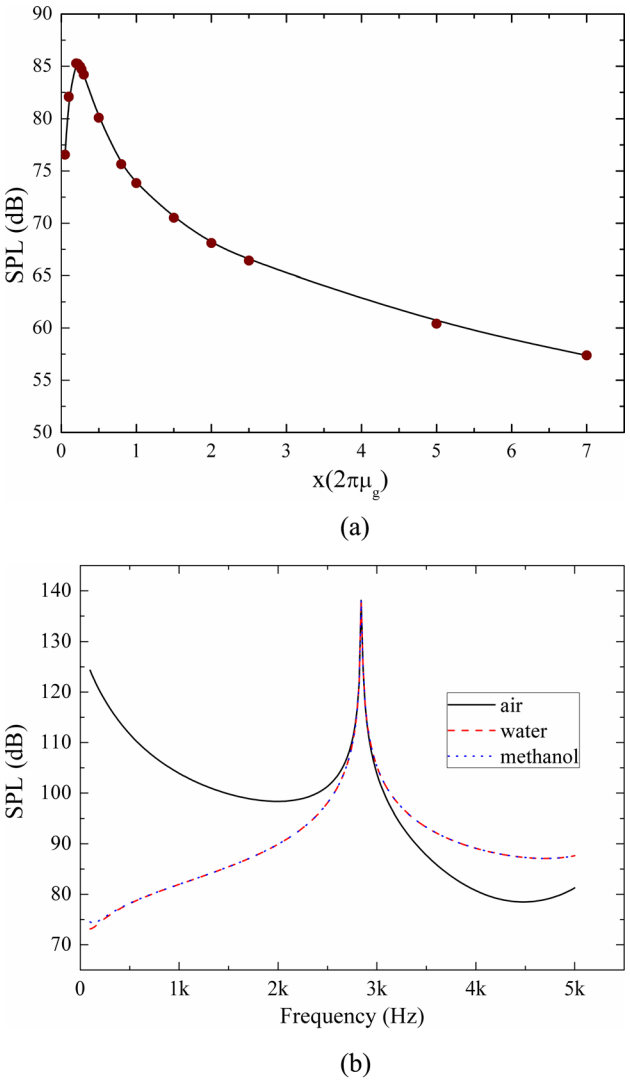

Fig. 5 Acoustic response for an encapsulated thermal-acoustic transducer (*a*) for a 1 mm thick titanium window at frequency of 1500 Hz with varying l_g (*b*) for different media in which the transducer is immersed and with distance equals to half of the thermal length and the thickness of titanium window is 125 μm. The titanium window area is 7.5 cm × 6.5 cm and the input power is 1 W.

8cm × 6cm for both the titanium window and silicon wafer window. The window–MWCNT sheet distance for the titanium and silicon wafer window chambers is always taken as half of the thermal length ($2\pi\mu_g$) of the temperature wave in the chamber.

It is obvious that resonance occurs for both transducers. The resonance frequencies are 3100 and 5400 Hz for the titanium transducer input frequencies lower than 6000 Hz. However, there exists only one resonance frequency, at 5000 Hz, for the silicon wafer transducer for input frequencies lower than 6000 Hz. The difference is mainly due to different material properties. For identical thermal and geometric boundary conditions, the resonance frequency of the silicon wafer plate is higher than that of the titanium plate. Therefore, the resonance frequency could be tailored by either material selection or by window dimensioning. The acoustic pressure decreases with increasing frequency for both transducers except at resonance. Hence, this transducer can be used as a resonator. From Fig. 4, it is observed that the acoustic pressure is very high at resonance, thus it can be used to either generate acoustic waves at specific frequencies or to select specific frequencies from a signal. In particular, if specific resonance frequencies can be chosen, it can be used as a musical instrument.

Referring to Eq. (22), it is noticed that the window–thin-film distance l_g is a very important parameter for the acoustic pressure. In this example, the titanium window transducer is chosen to illustrate the influence of this parameter on acoustic pressure. The relation of acoustic pressure with distance l_g is shown in Fig. 5(*a*). It is observed that there exists an extreme value located at a distance $0.2 \times 2\pi\mu_g$. The acoustics pressure decreases with increasing window–thin-film distance. For different transducers, the extreme value may be at different locations. Hence, to enhance the efficiency of a gas-filled encapsulated chamber transducer, a proper window–thin-film distance corresponding to the extreme acoustic pressure is recommended. It should be noted that the acoustic pressure is determined through an exact acoustic expression for a distance that is smaller than half of the thermal length.

The acoustic response as shown in Fig. 5(*b*) is affected by different media in which the transducer is immersed. The transducer is placed in a liquid medium with the window parallel to the liquid surface and the distance from the transducer (i.e., window) to liquid surface is 20 cm. It is noticed that resonance occurs for different media, while the acoustic pressure is very different for air and water. The response of methanol is almost the same as that of water. Thus the acoustic response outside the transducer is significantly affected by the medium in which the transducer is immersed. A gaseous medium shows a better performance at a

lower frequency with respect to the resonant frequency, while for liquid, a higher acoustic pressure is achieved at a higher frequency with respect to the resonant frequency.

4 Conclusion

A new model for a gas-filled encapsulated thermal-acoustic transducer is developed and exact and approximate solutions are derived. A comparison between analytical predictions and experimental results are presented and excellent agreement is reported. The frequency response for this acoustic transducer is investigated and the effect of window–thin film distance of the encapsulated transducer to the acoustic response is discussed. For a suitably chosen input frequency, resonance takes place and thus this kind of transducer can be used to either generate acoustic waves of specific frequency or to filter specific resonant frequencies from a wide spectrum of signal. To enhance conversion efficiency from electrical power to acoustic power, an optimal window–thin-film distance should be used. Because the window transmission coefficient influences acoustic pressure outside the chamber, the acoustic response is different for different transducer media. A gaseous medium results in a better performance at lower frequency while it is otherwise for a liquid medium. Although the different boundary conditions for forced window vibrations are slightly different from those of the experiment, the comparisons provide evidence that the model can be used as a guideline and information for enhancing efficiency conversion as well as for the design of a thermal-acoustic transducer. Finally, although a rectangular window is used in the examples presented, the analytical prediction derived is by all means not restrictive and it is applicable to all other window shapes. For instance, any circular window can be used in place of the rectangular window.

Acknowledgment

The work described in this paper was supported by the National Natural Science Foundation of China through a research grant awarded to the Shenzhen Research Institute, City University of Hong Kong (Project No. 11272271). The support of The Hong Kong Scholars Program 2011 is also acknowledged.

Nomenclature

C_m = isentropic sound velocity in the medium outside chamber
$C_T = P_0/\rho_0$ = isothermal sound velocity in gas
c_s = heat capacity per unit area
$j = \sqrt{-1}$ = imaginary unit
L = thickness of window
l_g = distance between the CNT film and the window
p_g = gas pressure
P_{in} = input power
P_0 = ambient pressure
$Q_0 = -\kappa_g \partial T_g(x,t)/\partial x\big|_{x=0}$ = instantaneous heat flow per unit area from thin film to surrounding medium
s = single-side area of CNT thin film
T = sound transmission coefficient of the window
T_f = temperature above CNT film's surroundings
T_g = varying temperature in chamber
T_m = average temperature in chamber
α_g = coefficient of thermal diffusivity in gas
β_0 = rate of heat loss per unit area of heated CNT film
κ_g = thermal conductivity of gas
γ = heat capacity ratio of gas
ρ_0 = reference gas density
ρ_m = density of the medium in which the transducer is immersed
ρ_w = density of window
ρ_g = gas density
ω = circular frequency
$\mu_g = \sqrt{2\alpha_g/\omega}$ = thermal diffusion length
υ = Poisson's ratio of window

Appendix A

A single-layer plate with thickness L and surrounded by two liquid media is shown in Fig. 6, where P_i is the incident acoustic pressure wave, P_r and P_t are the reflected and transmitted acoustic wave, respectively. For a normal incident wave, $\theta_1 = \theta_3 = 0$, and the transmission coefficient is [27]

$$T = \frac{2UZ_3}{V(Z_1 + Z_3) + j[(U^2 - V^2)Z_3 + Z_1]} \tag{A1}$$

where $U = (Z_2/Z_3)/\sin(-k_2L)$, $V = Z_2\cot(-k_2L)/Z_3$, $Z_i = \rho_i C_i$ $(i = 1,2,3)$, $k_2 = \omega/C_2$. It should be noted that $C_i (i = 1,2,3)$ represents the wave velocity in different media.

For example, consider a titanium single-layer plate with thickness of 125 μm, which is used in the study in this paper. The first and third media are argon and air, respectively. Substituting all material constants shown in Table 1 into Eq. (A1) yields the magnitude of transmission coefficient as 0.036 which is far smaller than 1. This verifies that the sound-hard boundary condition for pressure assumed in this paper is reasonable.

Appendix B

The window of an encapsulated chamber transducer undergoes forced vibration when an electrical power is applied to the nanotube thin film. The average chamber temperature increases when the nanotube thin film is heated. Hence a distributed force on the window results and it can be determined using the ideal gas law $q_0 = P_0\Delta T/T_0$, where P_0, T_0, and ΔT are the gas pressure, temperature, and temperature variation, respectively. Here the average temperature variation in the chamber is taken as $\Delta T = T_a/2$, where T_a is expressed in Eq. (17). For a rectangular plate (see Fig. 7) with four simply supported boundaries, the plate deflection is given by [28]

$$w = w_{\max}\sin\frac{\pi x}{a}\sin\frac{\pi y}{b} \qquad (0 < x < a, 0 < y < b) \tag{B1}$$

and the maximum deflection at the center of the plate is [28]

$$w_{\max} = \frac{16q_0a^4b^4}{D_0(a^2 + b^2)\pi^6} \tag{B2}$$

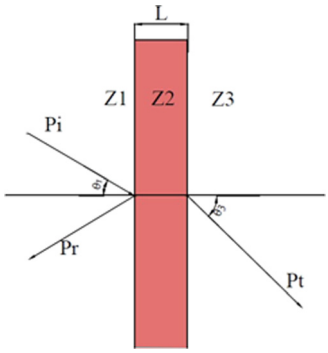

Fig. 6 Sound transmission through a plate

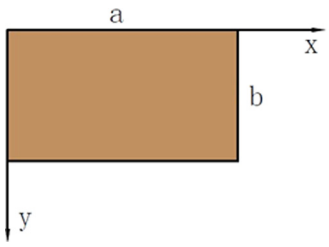

Fig. 7 The coordinate system and dimensions for a plate

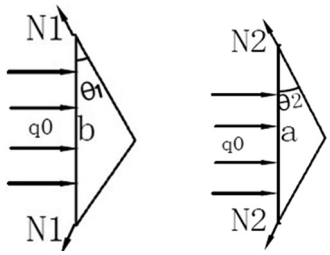

Fig. 8 Force equilibrium for the cross section of a plate

where $D_0 = Eh^3/[12(1-\upsilon^2)]$ is the plate flexural rigidity, h is the plate thickness, a and b are plate length and width, E and υ are Young's modulus and Poisson's ratio, respectively. The plate tension can be approximated by (see Fig. 8)

$$N_1 \approx \frac{q_0 b}{2\sin\theta_1}, \quad N_2 \approx \frac{q_0 a}{2\sin\theta_2} \tag{B3}$$

Assuming small plate deflection as compared to the other plate dimension, it can be shown that

$$\sin\theta_1 \approx \frac{2bw_x}{b^2+2w_x^2}, \quad \sin\theta_2 \approx \frac{2aw_y}{a^2+2w_y^2} \tag{B4}$$

where $w_x = w_{\max}\sin(\pi x/a), w_y = w_{\max}\sin(\pi y/b)$. Combining Eqs. (B3) and (B4) gives

$$N_1 = \frac{q_0 b^2}{4w_x} + q_0 w_x, \quad N_2 = \frac{q_0 a^2}{4w_y} + q_0 w_y \tag{B5}$$

The resonance frequency of the plate with in-plane force is [28]

$$\omega_{mn} = \sqrt{\frac{D_0}{\rho_w h}}\sqrt{\left[\left(\frac{m\pi}{a}\right)^2+\left(\frac{n\pi}{b}\right)^2\right]^2 + \frac{N_1}{D_0}\left(\frac{m\pi}{a}\right)^2 + \frac{N_2}{D_0}\left(\frac{n\pi}{b}\right)^2} \tag{B6}$$

When a variable, time-dependent load $p = p_0\exp(j\omega t)$ is applied on the plate, the transverse velocity of the plate under forced vibration is [29]

$$v = \frac{16p_0}{\rho_w h\pi^2}\sum_{m=1,3,\ldots}^{\infty}\sum_{n=1,3,\ldots}^{\infty}\frac{j\omega\exp(j\omega t) - j\omega_{mn}\exp(j\omega_{mn}t)}{mn\left(\omega_{mn}^2-\omega^2\right)} \times \sin\frac{m\pi}{a}x\sin\frac{n\pi}{b}y \quad (0<x<a, 0<y<b) \tag{B7}$$

Here, the amplitude of the applied load is $p_0 = \bar{p}_g(l_g)$. For a specific vibration mode (m,n), the velocity amplitude is small and its contribution to the acoustic pressure is omitted. Then the acoustic pressure generated by the mechanical window vibration can be expressed as

$$p_{vp}(x,t) = \bar{p}_{vp}(x)\exp(j\omega t) \tag{B8}$$

where

$$\bar{p}_{vp}(x) = \frac{64\rho_m C_m}{\rho_w h\pi^4}\sum_{m=1,3,\ldots}^{\infty}\sum_{n=1,3,\ldots}^{\infty}\frac{j\omega\bar{p}_g(l_g)}{m^2n^2\left(\omega_{mn}^2-\omega^2\right)} \times \exp\left(j\frac{\omega}{C_m}(l_g+L-x)\right) \tag{B9}$$

where ρ_m and C_m are density and acoustic velocity of the medium in which the transducer is immersed. It should be noticed that the averaged values for w_x and w_y are used to calculate the tension in Eq. (B5). Also, the averaged velocity in Eq. (B7) is taken to derive the acoustic pressure in Eq. (B9).

References

[1] Bédard, M., and Berry, A., 2008, "Development of a Directivity-Controlled Piezoelectric Transducer for Sound Reproduction," J. Sound Vib., **311**(3–5), pp. 1271–1285.

[2] Sun, J. Q., Norris, M. A., Rossetti, D. J., and Highfill, J. H., 1996, "Distributed Piezoelectric Actuators for Shell Interior Noise Control," ASME J. Vibr. Acoust., **118**(4), pp. 676–681.

[3] Preumont, A., Francois, A., and Dubru, S., 1999, "Piezoelectric Array Sensing for Real-Time, Broad-Band Sound Radiation Measurement," ASME J. Vibr. Acoust., **121**(4), pp. 446–452.

[4] Bailo, K. C., Brei, D. E., and Grosh, K., 2003, "Investigation of Curved Polymeric Piezoelectric Active Diaphragms," ASME J. Vibr. Acoust., **125**(2), pp. 145–154.

[5] Arnold, H. D., and Crandall, I. B., 1917, "The Thermophone as a Precision Source of Sound," Phys. Rev., **10**(1), pp. 22–38.

[6] Xiao, L., Chen, Z., Feng, C., Liu, L., Bai, Z.-Q., Wang, Y., Qian, L., Zhang, Y., Li, Q., Jiang, K., and Fan, S., 2008, "Flexible, Stretchable, Transparent Carbon Nanotube Thin Film Loudspeakers," Nano Lett., **8**(12), pp. 4539–4545.

[7] Venkatasubramanian, R., 2010, "Applied Physics: Nanothermal Trumpets," Nature, **463**(7281), pp. 619–619.

[8] Shinoda, H., Nakajima, T., Ueno, K., and Koshida, N., 1999, "Thermally Induced Ultrasonic Emission From Porous Silicon," Nature, **400**(6747), pp. 853–855.

[9] Liu, K., Sun, Y., Chen, L., Feng, C., Feng, X., Jiang, K., Zhao, Y., and Fan, S., 2008, "Controlled Growth of Super-Aligned Carbon Nanotube Arrays for Spinning Continuous Unidirectional Sheets With Tunable Physical Properties," Nano Lett., **8**(2), pp. 700–705.

[10] Aliev, A. E., Lima, M. D., Fang, S., and Baughman, R. H., 2010, "Underwater Sound Generation Using Carbon Nanotube Projectors," Nano Lett., **10**(7), pp. 2374–2380.

[11] Kozlov, M. E., Haines, C. S., Oh, J., Lima, M. D., and Fang, S., 2009, "Sound of Carbon Nanotube Assemblies," J. Appl. Phys., **106**(12), p. 124311.

[12] Tian, H., Ren, T.-L., Xie, D., Wang, Y.-F., Zhou, C.-J., Feng, T.-T., Fu, D., Yang, Y., Peng, P.-G., Wang, L.-G., and Liu, L.-T., 2011, "Graphene-on-Paper Sound Source Devices," ACS Nano, **5**(6), pp. 4878–4885.

[13] Niskanen, A. O., Hassel, J., Tikander, M., Maijala, P., Gronberg, L., and Helisto, P., 2009, "Suspended Metal Wire Array as a Thermoacoustic Sound Source," Appl. Phys. Lett., **95**(16), p. 163102.

[14] Vesterinen, V., Niskanen, A. O., Hassel, J., and Helistö, P., 2010, "Fundamental Efficiency of Nanothermophones: Modeling and Experiments," Nano Lett., **10**(12), pp. 5020–5024.

[15] Xiao, L., Liu, P., Liu, L., Li, Q., Feng, Z., Fan, S., and Jiang, K., 2011, "High Frequency Response of Carbon Nanotube Thin Film Speaker in Gases," J. Appl. Phys., **110**(8), p. 084311.

[16] Hu, H., Zhu, T., and Xu, J., 2010, "Model for Thermoacoustic Emission From Solids," Appl. Phys. Lett., **96**(21), p. 214101.

[17] Aliev, A. E., Lima, M. D., Fang, S., and Baughman, R. H., 2010, "Supporting Online Materials for Underwater Sound Generation Using Carbon Nanotube Projectors," Nano Lett., **10**(7), pp. 2374–2380.

[18] Lim, C. W., Tong, L. H., and Li, Y. C., 2013, "Theory of Suspended Carbon Nanotube Thin Film as a Thermal-Acoustic Source," J. Sound Vib. (in press).

[19] McDonald, F. A., and Wetsel, J. G. C., 1978, "Generalized Theory of the Photoacoustic Effect," J. Appl. Phys., **49**(4), pp. 2313–2322.

[20] Xiao, L. C. Z., Chen, Z., Feng, C., Liu, L., Bai, Z. Q., Wang, Y., Qian, L., Zhang, Y. Y., Li, Q., Jiang, K. L., and Fan, S., 2008, "Supporting Online Materials for Flexible, Stretchable, Transparent Carbon Nanotube Thin Film Loudspeakers," Nano Lett., **8**(12), pp. 4539–4545.

[21] Rosencwaig, A., and Gersho, A., 1976, "Theory of the Photoacoustic Effect With Solids," J. Appl. Phys., **47**(1), pp. 64–69.

[22] Hanping, H., Wang, Y., And Wang, Z., 2012, "Wideband Flat Frequency Response of Thermo-Acoustic Emission," J. Phys. D: Appl. Phys., **45**, p. 345401

[23] Aamodt, L. C., Murphy, J. C., and Parker, J. G., 1977, "Size Considerations in the Design of Cells for Photoacoustic Spectroscopy," J. Appl. Phys., **48**(3), pp. 927–933.

[24] Paul, O., and Baltes, H., 1999, "Mechanical Behavior and Sound Generation Efficiency of Prestressed, Elastically Clamped and Thermomechanically Driven Thin Film Sandwiches," J. Micromech. Microeng., **9**, pp. 19–29.

[25] Wikipedia, 2013, "Titanium," http://en.wikipedia.org/wiki/Titanium

[26] El-Cat, Inc., 2008, "Properties of Silicon and Silicon Wafers," http://www.phy.duke.edu/~hx3/physics/silicon/silicon.htm
[27] Barnard, G. R., Bardin, J. L., and Whiteley, J. W., 1975, "Acoustic Reflection and Transmission Characteristics for Thin Plates," J. Acoust. Soc. Am., **57**(3), pp. 577–584.
[28] Leissa, A. W., 1969, *Vibration of Plates, Scientific and Technical Information Division, National Aeronautics and Space Administration*, U.S. GPO, Washington, D.C.
[29] Ventsel, E., 2001, *Thin Plates and Shells: Theory, Analysis, and Applications*, Marcel Dekker, New York.